

Optical Engineering

OpticalEngineering.SPIEDigitalLibrary.org

Fiber-integrated tungsten disulfide saturable absorber (mirror) for pulsed fiber lasers

Hao Chen
Irene Ling Li
Shuangchen Ruan
Tuan Guo
Peiguang Yan

Fiber-integrated tungsten disulfide saturable absorber (mirror) for pulsed fiber lasers

Hao Chen,^a Irene Ling Li,^a Shuangchen Ruan,^a Tuan Guo,^b and Peiguang Yan^{a,*}

^aShenzhen University, College of Optoelectronic Engineering, Key Laboratory of Advanced Optical Precision Manufacturing Technology of Guangdong Higher Education Institutes, Shenzhen Key Laboratory of Laser Engineering, Nanhai Avenue 3688, Shenzhen 518060, China

^bJinan University, Institute of Photonics Technology, 601 Huangpu Avenue West, Guangzhou 510632, China

Abstract. We propose two schemes for achieving tungsten disulfide (WS₂)-based saturable absorber (SA) and saturable absorber mirror (SAM). By utilizing the pulsed laser deposition method, we grow the WS₂ film on micro-fiber to form an evanescent field interaction SA device. Incorporating this SA device into a common ring-cavity erbium-doped fiber (EDF) laser, stably passive mode-locking can be achieved with pulse duration of 395 fs and signal-to-noise ratio of 64 dB. We also produce a fiber tip integrated WS₂-SAM by utilizing the magnetron sputtering technique (MST). This new type of SAM combines the WS₂ layer as SA and gold mirror as high reflective mirror. By employing the WS₂-SAM, we construct the linear-cavity EDF lasers, and achieve passive mode-locking operation with pulse duration of ~1 ns and SNR of ~61 dB. We further achieve stably passive Q-switching operation with pulse duration of ~160 ns and pulse energy of 54.4 nJ. These fiber-integrated SAs and SAMs have merits of compactness and reliability, paving the way for the development of new photonic devices such as SAs for pulsed laser technology. © The Authors. Published by SPIE under a Creative Commons Attribution 3.0 Unported License. Distribution or reproduction of this work in whole or in part requires full attribution of the original publication, including its DOI. [DOI: [10.1117/1.OE.55.8.081318](https://doi.org/10.1117/1.OE.55.8.081318)]

Keywords: ultrafast lasers; fiber lasers; graphene; transition metal dichalcogenides.

Paper 151853SS received Jan. 4, 2016; accepted for publication Feb. 22, 2016; published online Mar. 29, 2016.

1 Introduction

Pulsed fiber lasers have attracted much attention owing to many potential applications in such areas as environmental sensing, biomedical diagnostics, and nonlinear frequency generation.^{1,2} Mainly two schemes are selected for generating pulsed laser emission—active mode-locking or Q-switching by employing costly and complex electrically driven modulators,^{3–5} and passive mode-locking or Q-switching by incorporating an artificial or real saturable absorber (SA) as an intensity-dependent optical switch. Compared with active scheme, passive scheme has the advantages of compactness, simplicity, and flexibility. In the past, the nonlinear polarization rotation (NPR), nonlinear optical loop mirror (NOLM),⁶ and semiconductor saturable absorber mirror (SESAM)⁷ were the dominant techniques with wide application in commercial laser system. Both NPR and NOLM are the fiber nonlinearity-based artificial SAs with higher damage threshold, but are also highly sensitive to environmental fluctuations. SESAM requires complicated fabrication and packaging process, and has limited bandwidth, few picoseconds response times. From the last decade, carbon nanotube (CNT)^{8–15} has emerged as the first case of nanomaterial SA for mode-locking, which has one-dimensional (1-D) nanostructure and owns advantages such as ultrafast photoresponse, easy fabrication, and low cost. Gold nanorod (GNR)^{16,17} is another familiar 1-D nanomaterial SA, which has two surface plasmon resonance absorption bands and has been utilized for Q-switching or mode-locking. These 1-D nanomaterial SAs have absorption peaks related with the tube diameter (for CNT) or the aspect

ratio (for GNR), thus leading to relatively narrowband operation restricted by the optimal absorption band. For wideband operation, the 1-D nanomaterial SAs require the combination of their nanotubes with a broad diameters distribution or nanorods with different aspect ratio. Unlike CNT or GNR, graphene^{18,19} has a Dirac-like electronic band structure with unique zero bandgap, which endows it with remarkable optical properties (i.e., ultrafast photoresponse, ultrabroadband absorption) and electrical properties (i.e., remarkable electron mobility). Extensively, research^{20–47} has employed graphene as a candidate material for the development of functional photonic technologies, e.g., ultrafast mode-locker, broadband polarizer, and phase shifter. But graphene also holds two main disadvantages, the weak modulation depth (typically ~1.3% per layer²⁰) and the difficulty of creating an optical bandgap. Therefore, substantial endeavors have been focused on developing new SA beyond graphene from other layered crystal,⁴⁸ such as topological insulators (TIs),^{49–82} transition metal dichalcogenides (TMDs),^{83–114} including of molybdenum disulfide (MoS₂) or tungsten disulfide (WS₂), as well as their diselenide analogues (MoSe₂, MoTe₂, WSe₂, and WTe₂) and black phosphorus.^{115–118} The series of TIs (i.e., Bi₂Te₃, Sb₂Te₃, Bi₂Se₃, and so on) demonstrate the characteristics of a small bandgap in the bulk state and a gapless metallic state in the edge/surface. Both the bulk- and nanostructured-TIs have been applied in pulsed laser cavity as the SA device. The TMDs possesses a thickness-dependent electronic and optical property—their bulk states have indirect bandgap with weak light–matter interaction while monolayer or few-layer structures are direct bandgap semiconductor with enhanced light activity. For example, a bulk WS₂ is a semiconductor with bandgap of 1.4 eV (0.886 μm), while its monolayer has a direct bandgap of 2.1 eV (0.59 μm). Its

*Address all correspondence to: Peiguang Yan, E-mail: yanpg@szu.edu.cn

thickness-dependent bandgap and electronic band structure endow it with many potential optical applications in optical fields that require strong light–matter interaction. These newly emerged two-dimensional (2-D) materials possess remarkable abilities in the field of optoelectronics and nonlinear photonics, such as broadband SA, high third-order nonlinear susceptibility, and ultrafast carrier dynamics.

Several methods have been used to obtain the TMD SAs, such as solution processing method,⁸⁴ evanescent field-interaction method,^{39,52} composite films composed of nanomaterial flakes in a polyvinyl alcohol (PVA) host,^{43,53} and the bottom-up growth techniques such as chemical vapor deposition (CVD),^{92,99} pulsed laser deposition (PLD),^{63–64} and the magnetron sputtering technique (MST).^{60–61} In the laser cavity, these SAs are usually pasted on fiber ferrules, or embedded in the air channels of photonic crystal fiber (PCF),^{30,36,67,77,108,119–124} or deposited on microfiber or side polished fiber (SPF).^{56,58,59} The fiber ferrule-type SAs have inherently short nonlinear interaction length. The composite films SAs could maintain the thermal stability of SA materials, but is vulnerable to destruction by high power operation. Moreover, it should be guaranteed that light must transmit through the SA materials. The PCF-based SAs can supply strong interaction effect and large nonlinear effect, but their fabrication processes are complicated according to the previous report.¹⁰⁸ The microfiber-based SAs are attractive for long light–matter interaction length, making such SAs as light modulator and high nonlinear device simultaneously. As in Ref. 52, Luo et al. demonstrated the combination of high nonlinearity induced by the real part of third-order nonlinear optical property in passively mode-locked fiber lasers with high-repetition rates. The SPF-based SAs have the merits of high power tolerance and longer light–matter interaction length, but the SPF requires accurate polishing technique and usually causes unwanted polarization-dependent insertion loss.^{56,58} CVD offers a scalable method for the production of monolayer or few-layer TMD (i.e., MoS₂ or WS₂), but the film growth is limited by the low nucleation rate on bare substrates, and pretreatment of the substrate is often necessary to seed the TMD growth. The PLD and MST can produce the film by irradiating the target placed under vacuum chamber, and the film can be directly deposited on the substrate (i.e., quartz glass substrate,⁸⁵ microfiber,⁶³ SPF,⁶¹ or fiber-tip⁸⁰).

In this paper, we propose two schemes for achieving new WS₂-based SA and SAM devices as shown in Fig. 1. By utilizing the PLD method, we grow the WS₂ film on microfiber to form an evanescent field interaction SA device as in Fig. 1(a), which would have the combined advantages from the strong nonlinear optical response in material together with the sufficiently long-range interaction length in fiber taper. Incorporating this SA device into a common ring-cavity erbium-doped fiber (EDF) laser, stably passive mode-locking can be achieved with pulse duration of 395 fs and signal-to-noise ratio of 64 dB. On the other hand, we produce a fiber tip integrated WS₂-SAM by utilizing the MST method. This new type of SAM combines the WS₂ layer as SA and gold mirror as high reflective mirror, as shown in Fig. 1(b). By employing the WS₂-SAM, we construct the linear-cavity EDF lasers, and achieve passive mode-locking operation with pulse duration of ~1 ns and SNR of ~61 dB. We further achieve stably passive Q-switching

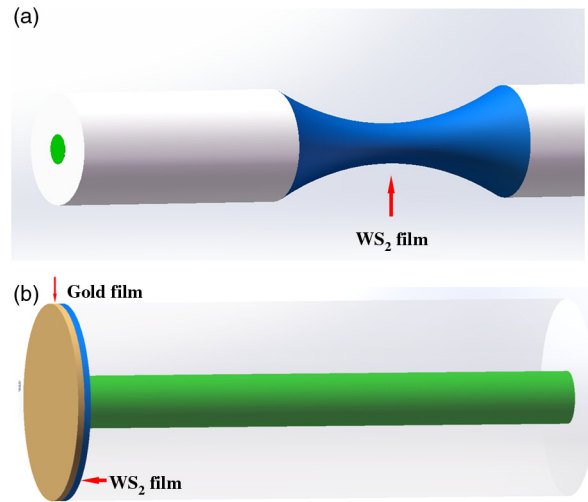


Fig. 1 (a) WS₂-SA integrated on microfiber and (b) WS₂-SAM integrated on fiber-tip.

operation with pulse duration of ~160 ns and pulse energy of 54.4 nJ. These fiber-integrated SAs and SAMs have merits of compactness and reliability. Our research, accompanied by studies from Bogusławski et al.,^{60,61} paves the way for the development of new photonic devices such as SAs for pulsed laser technology.

2 Fabrication, Characterization of Fiber-Integrated SA/SAM and Their Application in Pulsed Fiber Laser

2.1 Microfiber-Based WS₂-SA and its Application in Passively Mode-Locked EDF Laser

We employed the PLD method to fabricate the SA device. In this process, the WS₂ target was placed into a vacuum chamber where the vacuum degree was set at 5×10^4 Pa. A high energy Nd:YAG laser (SL II-10, Surelite) could emit 2 mJ/pulse laser beam, which was delivered into the chamber and focused on the target to inspire out of the plasma plume. When arrived to the microfiber, the W and S elements would grow on the side surface of microfiber. In the experiment, the deposition time was 2 h, and the deposition temperature was fixed at room temperature. To verify that the film was really deposited on microfiber, we executed a scanning electron microscope (SEM) on the WS₂ film morphology, as shown in Fig. 2. The waist region of microfiber had a diameter of ~16 μm . The guided light in taper region would effectively penetrate into the film and would be modulated along the microfiber. Figure 2(a) shows that a layer of WS₂ film clearly stuck tightly on the side of microfiber. The thickness of WS₂ film was measured to be ~1 μm . Figure 2(b) shows the film morphology. It illustrates that the film was quite different from the previously reported SA with relatively uniform size and thickness by LPE method.

For checking the Raman shift property of the as-prepared materials, the Raman spectra were measured by using a Raman spectrometer (LabRAM HR Evolution) with a laser at 514 nm. Figure 3(a) shows the measured Raman spectra of WS₂ film on quartz glass together with that of bare quartz glass. Notably, these peaks were also observed for the film with locations of LA(M) at 174 cm^{-1} , 2LA(M) at 350 cm^{-1} , E_{2g}¹ at 356 cm^{-1} and A_{1g} at 420.7 cm^{-1} , where

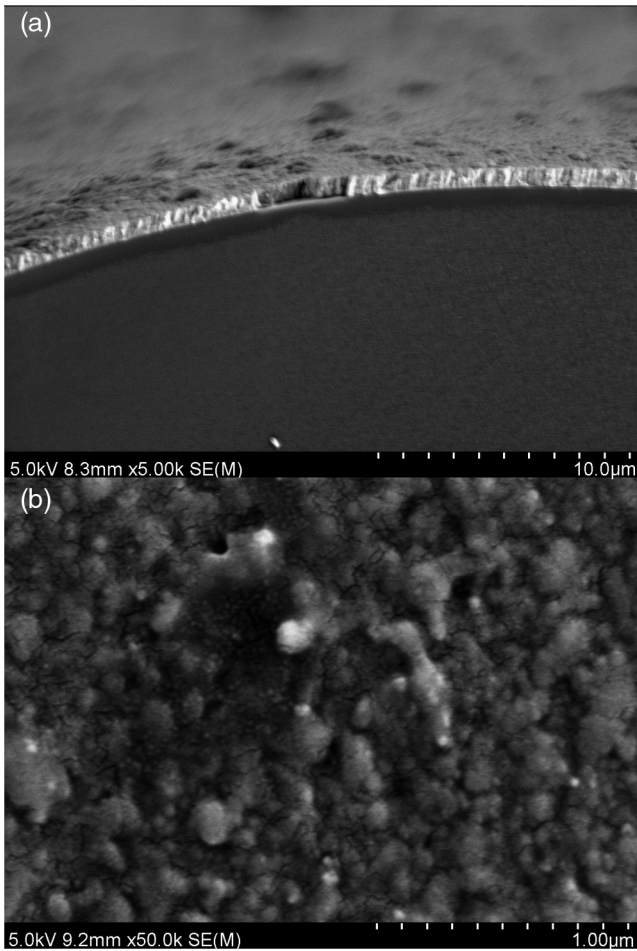


Fig. 2 SEM characteristic of the microfiber-based WS₂-SA. (a) WS₂ layer on fiber and (b) film morphology.

the LA(M) and 2LA(M) are the longitudinal acoustic modes, E_{2g}¹ is an in-plane optical mode, and A_{1g} corresponds to the out-of-plane vibrations along the *c*-axis direction of the S atoms.

We also measured the linear and nonlinear transmission of the SA device, as shown in Fig. 3(b). The linear transmission was at the level of 65.6% at 1560 nm by using an ASE source (Glight, 1250 to 1650 nm) and optical spectrum analyzer (OSA). The power-dependent nonlinear transmission is the key parameter to evaluate the mode-locking ability of SA. The SA of our fiber-integrated WS₂-SA was investigated by standard two-arm experiment. A homemade fs laser (central wavelength: 1562 nm, repetition rate: 22.5 MHz, pulse duration: 650 fs, average power: 12 mW) was utilized as test source, a variable optical attenuator was applied to continuously change the input optical intensity into the sample. A 50:50 optical coupler (OC) was used to split the laser into two arms with the 50% arm for power-dependent transmission measurement of SA device and the 50% arm for reference. A two-channel power meter with measuring range from 10 μW to 10 mW was used to measure the power. The modulation depth, saturation intensity, and nonsaturable loss were 7.8%, 189 MW/cm², and 25.7%, respectively. Furthermore, the SA might suffer from two-photon absorption as the transmittance declined when the intensity of input light exceeds around 450 MW/cm².

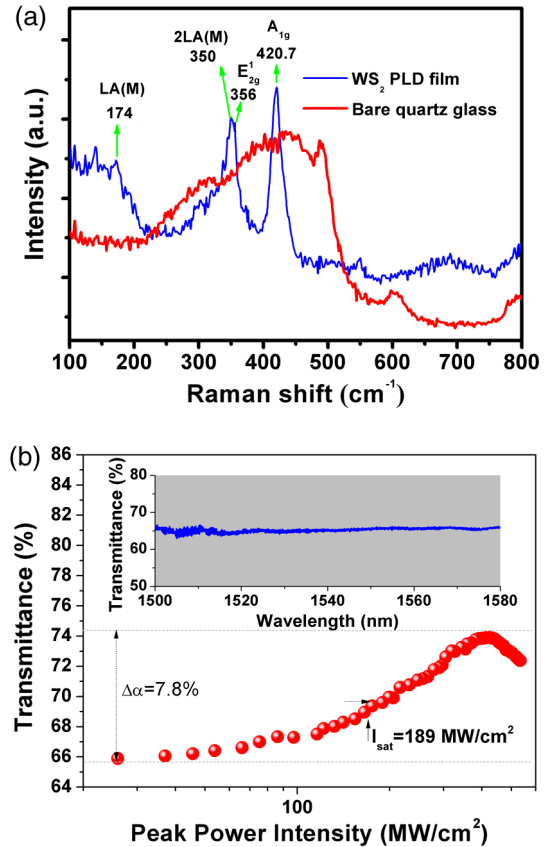


Fig. 3 (a) Raman spectra of bare quartz glass and WS₂ film on quartz glass. (b) Measured linear transmission (inset) and nonlinear transmission.

Figure 4 shows the schematic of mode-locked fiber laser with our WS₂-SA device. The pump source was a laser diode (LD) with emission centered at 974.5 nm. A piece of 2.4 m EDF was used as the laser gain medium with absorption coefficient of 25 dB/m at 980 nm (IsoGainTM I-25, Fibercore). The pump was delivered into EDF via a 980/1550 fused wavelength-division multiplexer (WDM) coupler. A polarization independent isolator (PI-ISO), placed after the EDF, was used to ensure unidirectional operation and eliminate undesired feedback from the output end facet. A fused fiber OC was used to extract 30% energy from the cavity. A polarization controller (PC), consisting of three spools of SMF-28 fiber, was placed in the ring cavity after the ISO. The WS₂-SA was inserted between the PC and the WDM coupler. Apart from the gain fiber, all the fiber devices in cavity were made by SMF-28 fiber. The laser performance

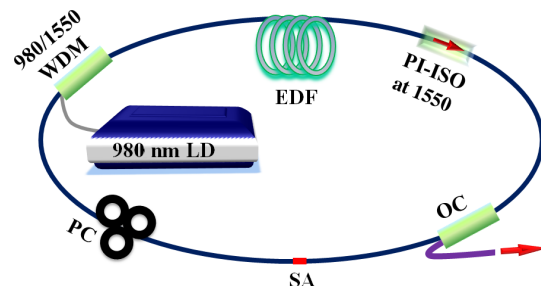


Fig. 4 Schematic of mode-locked fiber laser with WS₂-SA.

was observed using an OSA (Yokogawa, AQ6370B), 1 GHz digital oscilloscope (Tektronix, DPO7104C), 3 GHz RF spectrum analyzer (Agilent, N9320A) coupled with a 15 GHz photodetector (EOT, ET-3500FEXT), and an optical autocorrelator (APE, PulseCheck).

Figure 5(a) shows the typical spectrum of mode-locked pulses at the pump power of 65 mW. The generated optical soliton was centered at 1560 nm with a 3 dB spectral width of 6.75 nm. The appearance of pronounced Kelly sidebands indicated that the laser was in soliton operation. The radio frequency (RF) spectrum of the laser was shown in Fig. 5(b). The fundamental repetition frequency was 19.57 MHz with an SNR of 64 dB measured with a 1 kHz resolution bandwidth (RBW). Figure 5(c) shows the autocorrelation trace. It had a full width at half maximum

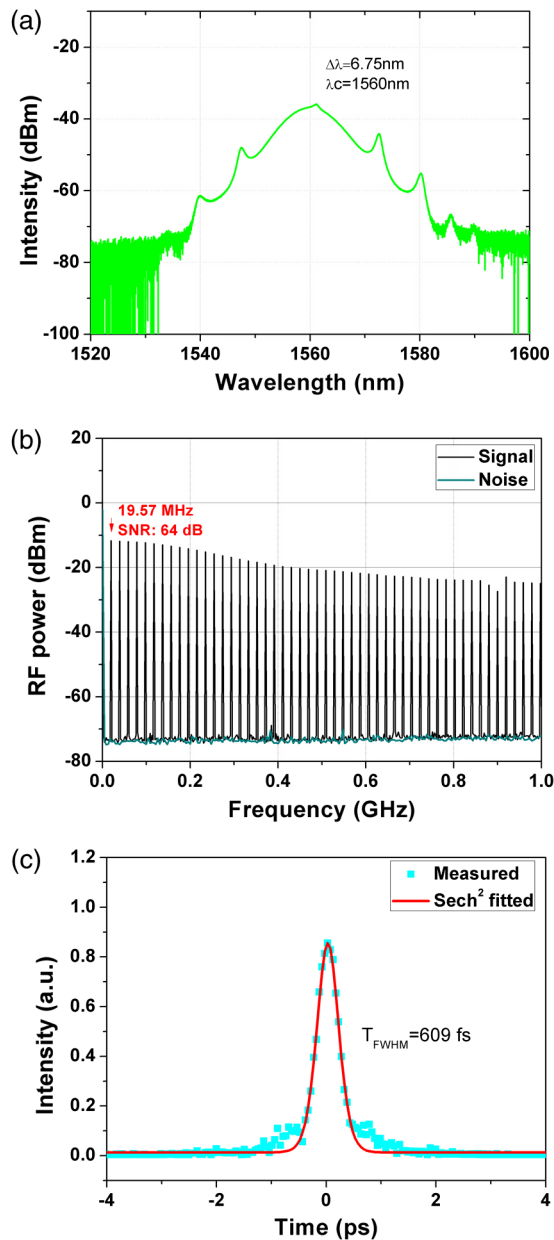


Fig. 5 Performance of mode-locked fiber laser. (a) Spectrum, (b) RF spectrum measured with a 1 kHz RBW, and (c) measured pulse duration.

(T_{FWHM}) of 609 fs, corresponding to pulse duration (Δt) of ~ 395 fs if a sech² pulse profile was assumed. The time-band product (TBP) was calculated to be 0.328 and deviated from the transform-limited value of 0.315, indicating that some chirp was included in the output pulse that had a broader bottom. The average output power was 1.5 mW, thus the output pulse energy was about 76.6 pJ.

2.2 Fiber-Tip-Integrated WS₂-SAM and its Application in Passively Mode-Locked and Q-Switched EDF Lasers

The MST was employed to fabricate the integrated WS₂-SAM. The WS₂ target was with the diameter of 49 mm, thickness of 3 mm, and purity of more than 99.5%. All the coating processes occurred in vacuum with the sputtering insert argon gas at pressure of 10³ Pa. During the deposition process, the AC voltage was applied to be 100 W in the chamber. The sputtered tungsten and sulfur atoms were ejected out from the target and then condensed on the fiber end. The synthesis lasted around 1 h at room temperature, forming a thin WS₂ film as the SA layer. Subsequently, the Au target was excited under the DC voltage for 3 min until the Au atoms formed a tightly thin film with thickness of ~ 150 nm on the SA layer. The gold film (GF) here not only functioned as a high reflective mirror, but also as a protective barrier that isolated the inner SA layer from the contamination, corrosion, and oxidation. Figure 6(a) shows the three-dimensional (3-D) view of the fabricated sample by confocal scanning microscopy. It indicated that the device was compact. To testify whether the SA was grown on the fiber end, we took out several samples from the chamber before the Au-film fabrication, which was direct deposited WS₂ film on pollution-free quartz glasses in the same conditions as production WS₂-SAM. Figure 6(b) shows the SEMs of the as-prepared sample at different scales. It illustrates that a layer of WS₂ film was successively deposited on the quartz glass. The film was composed by thin layer of nanoparticles with diameters from 10 nm to around 40 nm, thus we can deduce that the WS₂ film were also deposited on the fiber tip.

The Raman spectrum of the as-grown WS₂ was measured by a Raman spectrometer (LabRAM HR Evolution) with laser at 488 nm. Figure 7(a) shows the characteristic Raman bands, e.g., two optical phonon modes (E_{2g}^1 at 356 cm⁻¹ and A_{1g} at 417.5 cm⁻¹) and typical longitudinal acoustic modes 2LA(M) at 349.8 cm⁻¹, where the E_{2g}^1 is an in-plane optical mode and A_{1g} corresponds to the out-of-plane vibrations along the c -axis direction of the S atoms. The main Raman bands agreed with the earlier reports. The linear transmission of the sample was measured in the range from 1000 to 2000 nm by using an ASE source and OSA. It was at the level of $92.8 \pm 0.6\%$, and the transmittance at 1560 nm was 93.1%, as shown in Fig. 7(b). The nonlinear absorption curve gave a modulation depth of $\sim 4.48\%$, saturation intensity of ~ 138 MW/cm², and nonsaturable loss of 2%, as shown in Fig. 7(b). The nonsaturable loss here might be the smallest value when compared with other WS₂-SA reported in Refs. 103 and 105. We tend to believe that this remarkable improvement comes from the compactness of our device—no extra insertion loss is imported in this SAM. This design can allow the reflectivity up to 98%

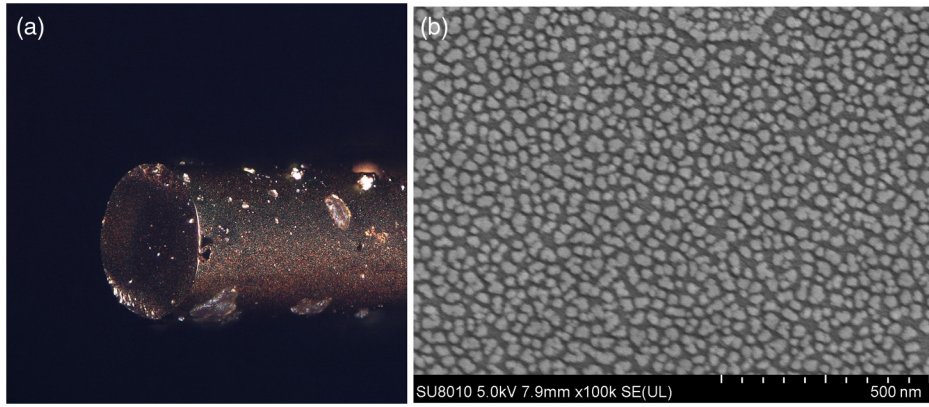


Fig. 6 (a) 3-D image of WS₂-SAM and (b) SEM of deposited WS₂ film.

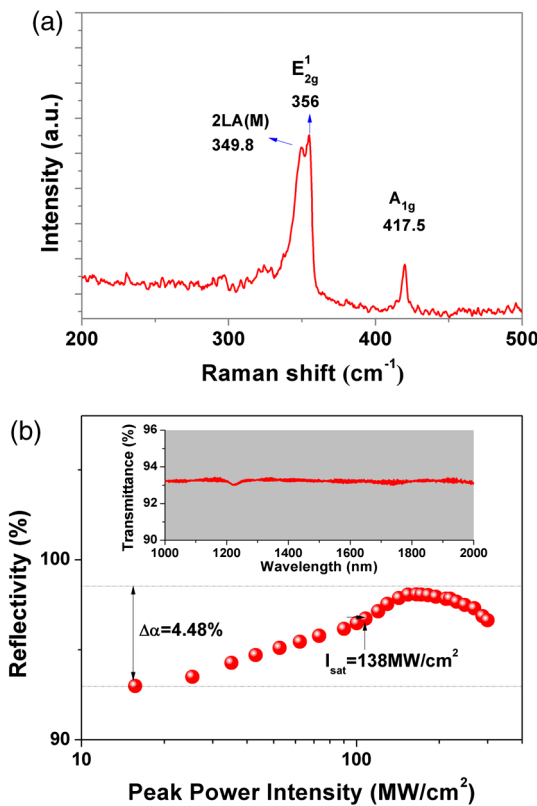


Fig. 7 (a) Raman spectra of WS₂ film. (b) Measured linear transmission (inset) and nonlinear transmission.

after the SA layer is saturable and only Au film is remained as a high reflective mirror.

A simplest linear cavity was implemented to obtain self-starting mode-locking operation, as shown in Fig. 8. The pump source was a 976 nm LD with maximum output power of 410 mW. A 980/1550 nm WDM was utilized to deliver the 976 nm pump light into the laser cavity and extract the laser output. The cavity was constructed by fiber Bragg grating (FBG), EDF, and WS₂-SAM. An FBG centered at 1560 nm was utilized as output coupler with 3-dB bandwidth of 0.2 nm and reflectivity of 88.52%. A 13 cm EDF (Liekki 110-4/125) was used as active media with absorption coefficient of 250 dB/m at 980 nm. The WS₂-SAM, serving as a light modulator and high reflective mirror, was spliced directly with the EDF. The other fibers in cavity were single mode fiber (Corning, SMF-28) with 16.2-cm length. At the output end, an isolator was added to eliminate undesired feedback from the output end facet.

The CW lasing state started to occur around the pump power of 6 mW, and the mode-locking operation would self-start and quickly stabilize when the pump power was beyond 30 mW. Figure 9 shows the measured spectrum, RF spectra, and pulse traces of the laser at the pump power of 410 mW. Figure 9(a) shows the spectrum of mode-locked pulses. The generated pulses are centered at 1560 nm with a 3-dB bandwidth of 0.031 nm. The mode-locking operated at a fundamental frequency of 352 MHz, corresponding well to the cavity round trip time. The RF spectrum in a 2 GHz span was also measured with RBW of 10 kHz and SNR of ~61 dB, as displayed in Fig. 9(b),

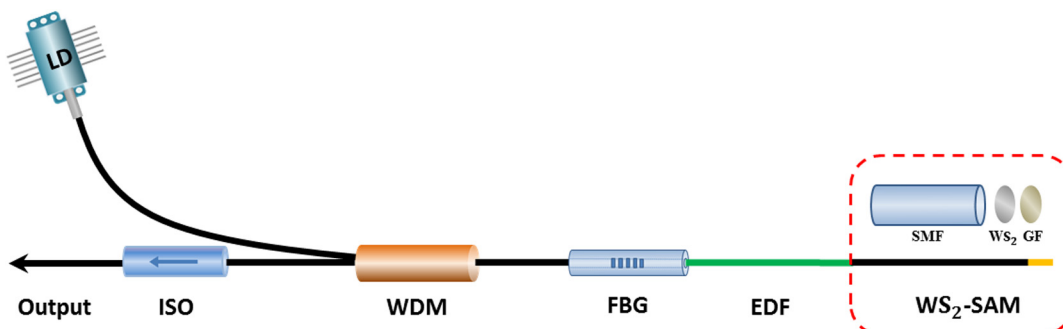


Fig. 8 Schematic of mode-locked fiber laser with WS₂-SAM.

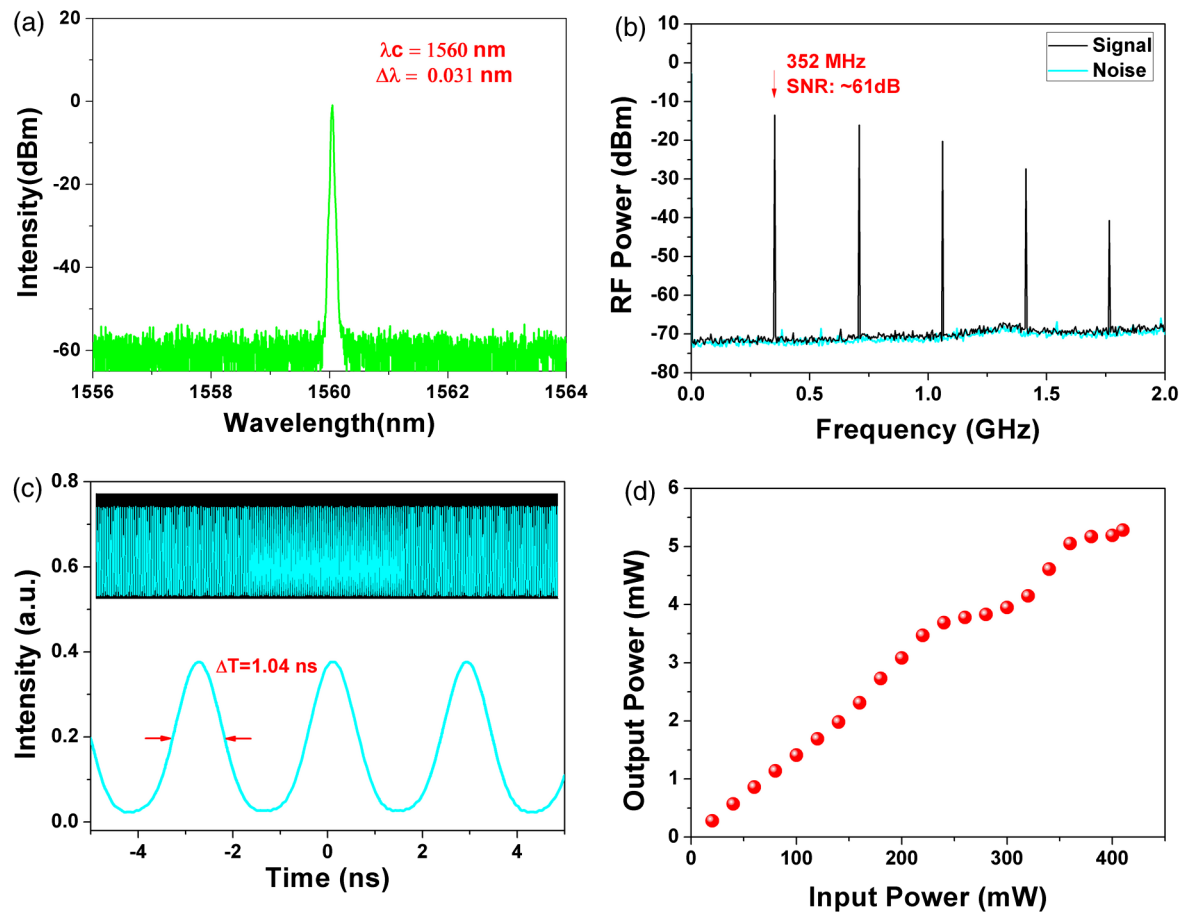


Fig. 9 Performance of mode-locked fiber laser. (a) Spectrum, (b) RF spectrum measured with a 10 kHz RBW, (c) measured pulse duration and pulse trace, and (d) output power versus input power.

certifying the stability of this mode-locking EDFL. Restricted by the bandwidth of our FBG, the output pulse had a width to be 1.04 ns, as shown in Fig. 9(c). Its long range stability had been characterized in a span of $1 \mu\text{s}$ by the inset. In the full pump range, the fundamental mode-locking state remained stable and no pulse-breaking and harmonic waves were observed on the oscilloscope. The power characteristic curve was shown in Fig. 9(d). It can be seen that the maximum output was 5.28 mW at 1560 nm.

It was noted that no PC was inserted into the cavity for stabilizing the pulse, unlike that in Ref. 100. Also, the pump threshold was much lower than the mode-locking EDFL based on MoS_2 -PVA SA.¹⁰⁰ This is because that the high reflection of narrowband FBG and WS_2 -SAM was beneficial to the rapid growth of cavity energy. As a fiber-integrated photonic device, this SAM also demonstrated well-thermal stability as the EDFLs worked at the maximum pump power. It was interesting that the generated pulse was restricted in the ns regime in our experiment, which might come from the inherent property of WS_2 nanoparticles. It was expected that the shorter pulse could be generated when the quality of WS_2 film was improved by optimizing the deposition condition and applying the postprocessing.

The deposition condition and integrated fiber type would have great impact on the laser performance. Apart from the above WS_2 -SAM sample, we also integrated the WS_2 -SAM on a polarization-maintaining fiber (PMF, PM980). Before

the deposition, the vacuum pressure specification in chamber was settled to 10^{-3} Pa to remove various impurity gases. During the deposition, the RF power was fixed at 100 W. The SMF tips were coated with a thin WS_2 nanomaterial functioned as SA layer during 1.5-h deposition process. Then the gold film was deposited under direct-current magnetron sputtering at the power of 80 W with ~ 300 -nm thickness.

In this case, the same linear-cavity structure was implemented to obtain the pulse operation by the WS_2 -SAM on PMF, whereas the EDF was replaced by 23-cm length of Liekki 110-4/125 and the total cavity was 44-cm long. It was very interesting that the fiber laser could easily achieve the stable Q-switched pulse output at such a simple structure. The laser performance was measured and shown in Fig. 10. The Q-switched pulse started to occur around the pump power of 50 mW, and then the Q-switched operation would maintain stably even the pump power up to 600 mW. Figures 10(a) and 10(b) show the measured optical spectrum and RF spectrum at pump power of 450 mW. It can be seen that the central wavelength was at 1560 nm with a 3-dB bandwidth of 0.025 nm, while the fundamental frequency was at 296.7 kHz with an RF SNR of 40 dB under RBW of 1 kHz. Figure 10(c) plotted the typical Q-switched pulse trains. At pump of 50 mW, the pulses had an FWHM of ~ 750 ns. The duration of Q-switched pulses decreased when the pump power increased, which was agreed with Q-switching properties. At the maximum pump of 600 mW,

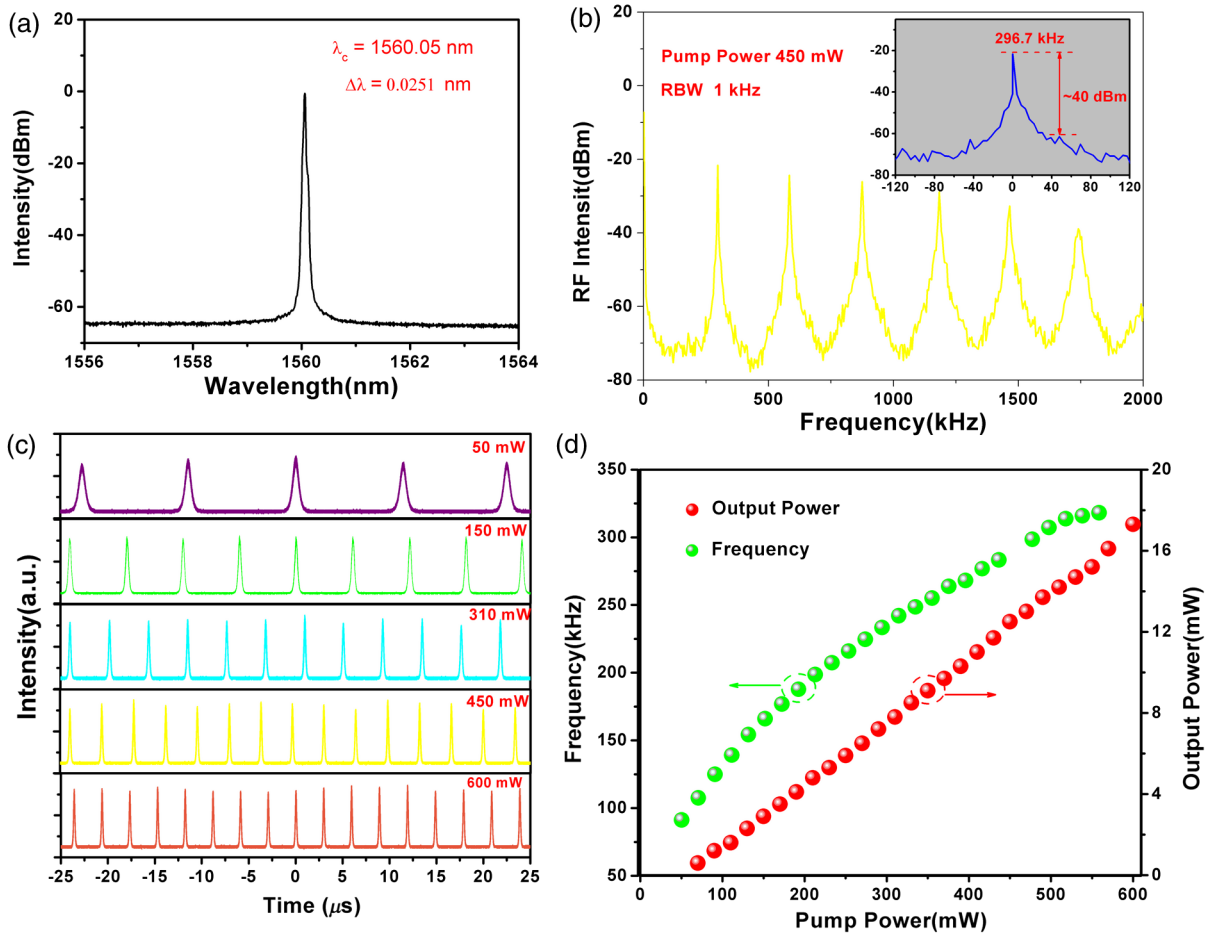


Fig. 10 Performance of Q-switched fiber laser. (a) Spectrum, (b) RF spectrum measured with a 1 kHz RBW, (c) measured pulse traces, and (d) output power versus input power.

the minimum pulse width was measured to be ~ 160 ns. Figure 10(d) shows the repetition rate and output power versus pump power. The repetition rate varied with a wide range from 91 to 318 kHz as a function of pump power. It was interesting to see that the output power almost linearly increased even when the pump power was up to 600 mW, indicating that the SAM functioned well without any extra protection at this pump level. The maximum output power was 17.3 mW, corresponding to the pulse energy of 54.4 nJ.

For the direct comparison with the previous works using CNT/graphene/TI as Q-switcher in EDF laser, we summarized their Q-switched pulse parameters, as listed in Table 1. It is notable that our work has the largest output power or

pulse energy; meanwhile, the pulse width of 160 ns is the shortest for the Q-switched EDFL with linear-cavity structure. It is expected that the pulse duration can be further shortened down to 100 ns by decreasing the length of the laser cavity and employing the high absorption gain fiber pumped by high power LD at 980 nm.

3 Conclusions

In summary, the fiber-integrated WS_2 -based SA and SAM were fabricated with the interesting merits of compactness and reliability. The compactness of these devices can effectively reduce their insertion loss, thus lowering the pump

Table 1 Parameters of Q-switched EDFLs using CNT/graphene/TI and WS_2 -SAM.

SA type	Operating wavelength (nm)	Cavity length (cm)	Frequency range (kHz)	Pulse width (ns)	Pulse energy (nJ)	References
	1534.1	10.5	~ 55 to 143.5	662	0.91	13
CNT	1534.1	110	14.5 to 141.4	330	7.3	12
Graphene	1538.3	37	31.7 to 236.3	206	33.2	125
Tl	1543.2	65	12.6 to 177.7	217	7.5	55
WS_2 -SAM	1560	44	91 to 318	160	54.4	This work

threshold for mode-locking or Q-switching. For the case of WS₂-SAM, the nonsaturable loss can be regarded as nearly negligible after the SA layer was saturable. The suppression of unwanted loss (both the insertion loss and nonsaturable loss) allows these devices to possess more reliable performance than those CNT/graphene/TIs sandwiched between fiber connectors. For the WS₂-SAM in experiment, no scheme was applied to protect them from the thermal damage. Once the Q-switching state self-started, it would remain stable even at the maximum power of 600 mW, and occur repeatedly with the booting of pump LD. It is believed that the fiber-integrated SAM can serve as a candidate practical SAM operating at watt-level pump.

As the library of 2-D materials grows, a number of studies emerge to produce and characterize SAs using heterostructures¹²⁶ or graphene and TMD-polymer composite.¹²⁷ New exotic properties are likely to emerge when different materials are combined. Unlike the inkjet printing method, the fabrication technique of WS₂-based SA or SAM can be applied to materials of other TMDs and the TI series. Both the PLD and PVD technologies allow the control over the ratio of different elements in the fabricated 2-D material film, and also allow the grown of different 2-D materials to build superlattice that can be artificially engineered their bandgap and thickness. However, substantial endeavors still need to improve the fiber-integrated WS₂-SA or SAM in the development of pulsed fiber lasers, especially to find the optimized deposition condition in the fabrication procedure, e.g., the deposition temperature and time, the lattice match of different SA materials.

Acknowledgments

This work was supported by the National Natural Science Foundation of China (Nos. 61205080 and 61308049), the Natural Science Fund of Guangdong Province (2014A030313387), the Science and Technology Project of Shenzhen City (JCYJ20140418091413568, 20140418095735582, JCYJ20150324140036862, JCYJ20130329142116637, JCYJ20150324140036870, and JCYJ20140418091413577), and the Youth Science and Technology Innovation Talents of Guangdong (No. 2014TQ01X539).

References

- X. Liu et al., "Distributed ultrafast fibre laser," *Sci. Rep.* **5**, 9101 (2015).
- X. Liu and Y. Cui, "Flexible pulse-controlled fiber laser," *Sci. Rep.* **5**, 9399 (2015).
- H. Chen et al., "Flexible rectangular wave-breaking-free pulse generation in actively mode-locked ytterbium-doped fiber laser," *Opt. Express* **22**(22), 26449–26456 (2014).
- H. Chen et al., "All fiber actively mode-locked ytterbium-doped laser with large range temporal tunability," *IEEE Photonics Technol. Lett.* **26**(17), 1786–1789 (2014).
- H. Chen et al., "Versatile long cavity widely tunable pulsed Yb-doped fiber laser with up to 27655th harmonic mode locking order," *Opt. Express* **23**(2), 1308–1318 (2015).
- H. Chen et al., "0.4 μ J, 7 kW ultrabroadband noise-like pulse direct generation from an all-fiber dumbbell-shaped laser," *Opt. Lett.* **40**(23), 5490–5493 (2015).
- U. Keller et al., "Semiconductor saturable absorber mirrors (SESAM's) for femtosecond to nanosecond pulse generation in solid-state laser," *IEEE J. Sel. Top. Quantum Electron.* **2**, 435–453 (1996).
- S. Yamashita et al., "Saturable absorbers incorporating carbon nanotubes directly synthesized onto substrates and fibers and their application to mode-locked fiber lasers," *Opt. Lett.* **29**, 1581–1583 (2004).
- F. Wang et al., "Wideband tuneable, nanotube mode-locked, fibre laser," *Nat. Nanotechnol.* **3**, 738–742 (2008).
- X. M. Liu et al., "Versatile multiwavelength ultrafast fiber laser mode-locked by carbon nanotubes," *Sci. Rep.* **3**, 2718 (2013).
- M. Zhang et al., "Mid-infrared Raman-soliton continuum pumped by a nanotube-mode-locked sub-picosecond Tm-doped MOPFA," *Opt. Express* **21**, 23261 (2013).
- B. Dong et al., "Wide pulse-repetition rate range tunable nanotube Q-switched low threshold erbium-doped fiber laser," *IEEE Photonics Technol. Lett.* **22**(24), 1853–1855 (2010).
- B. Dong et al., "Short linear-cavity Q-switched fiber laser with a compact short carbon nanotube based saturable absorber," *Opt. Fiber Technol.* **17**(2), 105–107 (2011).
- X. Li et al., "Nonlinear absorption of SWNT film and its effects to the operation state of pulsed fiber laser," *Opt. Express* **22**, 17227–17235 (2014).
- J. Z. Wang et al., "Pulse dynamics in carbon nanotube mode-locked fiber lasers near zero cavity dispersion," *Opt. Express* **23**, 9947–9958 (2015).
- Z. Kang et al., "Passively mode-locking induced by gold nanorods in erbium-doped fiber lasers," *Appl. Phys. Lett.* **103**, 041105 (2013).
- Z. Kang et al., "Passively mode-locked fiber lasers at 1039 and 1560 nm based on a common gold nanorod saturable absorber," *Opt. Mater. Express* **5**, 794–801 (2015).
- Q. L. Bao et al., "Atomic layer graphene as saturable absorber for ultrafast pulsed laser," *Adv. Funct. Mater.* **19**(19), 3077–3083 (2009).
- T. Hasan et al., "Nanotube-polymer composites for ultrafast photonics," *Adv. Mater.* **21**(38–39), 3874–3899 (2009).
- A. Martinez and Z. Sun, "Nanotube and graphene saturable absorbers for fibre lasers," *Nat. Photonics* **7**, 842–845 (2013).
- H. Zhang et al., "Large energy mode locking of an erbium-doped fiber laser with atomic layer graphene," *Opt. Express* **17**, 7630–7635 (2009).
- H. Zhang et al., "Large energy soliton erbium-doped fiber laser with a graphene-polymer composite mode locker," *Appl. Phys. Lett.* **95**(14), 141103 (2009).
- Z. Q. Luo et al., "Graphene-based passively Q-switched dual-wavelength erbium-doped fiber laser," *Opt. Lett.* **35**, 3709–3711 (2010).
- H. Zhang et al., "Graphene mode locked, wavelength-tunable, dissipative soliton fiber laser," *Appl. Phys. Lett.* **96**(11), 111–112 (2010).
- Q. Bao et al., "Graphene-polymer nanofiber membrane for ultrafast photonics," *Adv. Funct. Mater.* **20**(5), 782–791 (2010).
- Q. L. Bao and K. P. Loh, "Graphene photonics, plasmonics, and broadband optoelectronic devices," *ACS Nano* **6**, 3677–3694 (2012).
- H. Zhang et al., "Z-scan measurement of the nonlinear refractive index of graphene," *Opt. Lett.* **37**(11), 1856–1858 (2012).
- M. Zhang et al., "Tm-doped fiber laser mode-locked by graphene-polymer composite," *Opt. Express* **20**, 25077–25084 (2012).
- J. Ma et al., "Graphene mode-locked femtosecond laser at 2 μ m wavelength," *Opt. Lett.* **37**, 2085–2087 (2012).
- Y. H. Lin et al., "Using graphene nano-particle embedded in photonic crystal fiber for evanescent wave mode-locking of fiber laser," *Opt. Express* **21**, 16763–16776 (2013).
- S. Jaroslaw et al., "Simultaneous mode-locking at 1565 nm and 1944 nm in fiber laser based on common graphene saturable absorber," *Opt. Express* **21**, 18994–19002 (2013).
- G. Sobon, J. Sotor, and K. M. Abramski, "Passive harmonic mode-locking in Er-doped fiber laser based on graphene saturable absorber with repetition rates scalable to 2.22 GHz," *Appl. Phys. Lett.* **100**, 161109 (2012).
- J. Q. Zhao et al., "Graphene-oxide-based q-switched fiber laser with stable five-wavelength operation," *Chin. Phys. Lett.* **29**(11), 114206 (2012).
- S. S. Huang et al., "Tunable and switchable multi-wavelength dissipative soliton generation in a graphene oxide mode-locked Yb-doped fiber laser," *Opt. Express* **22**, 11417–11426 (2014).
- Y. Meng et al., "Multiple-soliton dynamic patterns in a graphene mode-locked fiber laser," *Opt. Express* **20**(6), 6685–6692 (2012).
- J. Q. Zhao et al., "Cladding-filled graphene in a photonic crystal fiber as a saturable absorber and its first application for ultrafast all-fiber laser," *Opt. Eng.* **52**(10), 106105 (2013).
- H. Ahmad et al., "Photonic crystal fiber based dual-wavelength Q-switched fiber laser using graphene oxide as a saturable absorber," *Appl. Opt.* **53**(16), 3581–3586 (2014).
- S. S. Huang et al., "Soliton rains in a graphene-oxide passively mode-locked ytterbium-doped fiber laser with all-normal dispersion," *Laser Phys. Lett.* **11**, 025102 (2014).
- A. P. Luo et al., "Microfiber-based, highly nonlinear graphene saturable absorber for formation of versatile structural soliton molecules in a fiber laser," *Opt. Express* **22**, 27019–27025 (2014).
- S. S. Huang, Y. G. Wang, and P. G. Yan, "High-order harmonic mode locking in an all-normal dispersion Yb-doped fiber laser with a graphene-oxide saturable absorber," *Laser Phys.* **24**(1), 015001 (2014).
- R. Y. Lin et al., "Bright- and dark-square-pulse generated from a graphene-oxide mode-locked ytterbium-doped fiber laser," *IEEE Photonics J.* **6**(3), 1 (2014).
- Y. Meng et al., "16.1 μ m high-order passive harmonic mode locking in a fiber laser based on graphene saturable absorber," *Opt. Express* **22**(24), 29921–29926 (2014).

43. J. Q. Zhao et al., "An L-band graphene-oxide mode-locked fiber laser delivering bright and dark pulses," *Laser Phys.* **23**(7), 075105 (2013).
44. J. Q. Zhao, P. G. Yan, and S. C. Ruan, "Observations of three types of pulses in an erbium-doped fiber laser by incorporating a graphene saturable absorber," *Appl. Opt.* **52**, 8465–8470 (2013).
45. K. Wu et al., "Towards low timing phase noise operation in fiber lasers mode locked by graphene oxide and carbon nanotubes at 1.5 μm ," *Opt. Express* **23**(1), 501 (2015).
46. X. T. Gan et al., "Graphene-assisted all-fiber phase shifter and switching," *Optica* **2**, 468–471 (2015).
47. X. Li et al., "High-power graphene mode-locked Tm/Ho co-doped fiber laser with evanescent field interaction," *Sci. Rep.* **5**, 16624 (2015).
48. A. K. Geim and I. V. Grigorieva, "Van der Waals heterostructures," *Nature* **499**, 419–425 (2013).
49. C. Zhao et al., "Wavelength-tunable picosecond soliton fiber laser with topological insulator: Bi_2Se_3 as a mode locker," *Opt. Express* **20**(25), 27888–27895 (2012).
50. S. Lu et al., "Third order nonlinear optical property of Bi_2Se_3 ," *Opt. Express* **21**(2), 2072–2082 (2013).
51. Z. Q. Luo et al., "1.06 μm Q-switched ytterbium-doped fiber laser using few-layer topological insulator Bi_2Se_3 as a saturable absorber," *Opt. Express* **21**, 29516–29522 (2013).
52. Z. C. Luo et al., "2 GHz passively harmonic mode-locked fiber laser by a microfiber-based topological insulator saturable absorber," *Opt. Lett.* **38**, 5216–5219 (2013).
53. H. Liu et al., "Femtosecond pulse generation from a topological insulator mode-locked fiber laser," *Opt. Express* **22**, 6868–6873 (2014).
54. M. Liu et al., "Dual-wavelength harmonically mode-locked fiber laser with topological insulator saturable absorber," *IEEE Photonics Technol. Lett.* **26**, 983–986 (2014).
55. M. Wu et al., "Nanosecond-switched erbium-doped fiber laser with wide pulse-repetition-rate range based on topological insulator," *IEEE J. Quantum Electron.* **50**(6), 393–396 (2014).
56. J. Koo et al., "Passively Q-switched 1.56 μm all-fiberized laser based on evanescent field interaction with bulk-structured bismuth telluride topological insulator," *J. Opt. Soc. Am. B* **31**(9), 2157–2162 (2014).
57. Y. Chen et al., "Large energy, wavelength widely tunable, topological insulator Q-switched erbium-doped fiber laser," *IEEE J. Sel. Top. Quantum Electron.* **20**(5), 315–322 (2014).
58. J. Lee et al., "A femtosecond pulse erbium fiber laser incorporating a saturable absorber based on bulk-structured Bi_2Te_3 topological insulator," *Opt. Express* **22**(5), 6165–6173 (2014).
59. J. Sotor et al., "Mode-locked erbium-doped fiber laser based on evanescent field interaction with Sb_2Te_3 topological insulator," *Appl. Phys. Lett.* **104**(25), 251112 (2014).
60. J. Boguslawski et al., "Investigation on pulse shaping in fiber laser hybrid mode-locked by Sb_2Te_3 saturable absorber," *Opt. Express* **23**, 29014–29023 (2015).
61. J. Boguslawski et al., "Dissipative soliton generation in Er-doped fiber laser mode-locked by Sb_2Te_3 topological insulator," *Opt. Lett.* **40**(12), 2786–2789 (2015).
62. Y. H. Lin et al., "Using n- and p-type Bi_2Te_3 topological insulator nanoparticles to enable controlled femtosecond mode-locking of fiber lasers," *ACS Photonics* **2**(4), 481–490 (2015).
63. P. G. Yan et al., "A 2.95 GHz, femtosecond passive harmonic mode-locked fiber laser based on evanescent field interaction with topological insulator film," *Opt. Express* **23**(1), 154–164 (2015).
64. P. G. Yan et al., "A practical topological insulator saturable absorber for mode-locked fiber laser," *Sci. Rep.* **5**, 8690 (2015).
65. W. J. Liu et al., "Generation of dark solitons in erbium-doped fiber lasers based Sb_2Te_3 saturable absorbers," *Opt. Express* **23**, 26023–26031 (2015).
66. L. N. Duan et al., "Passively harmonic mode-locked fiber laser with a high signal-to-noise ratio via evanescent-light deposition of bismuth telluride topological insulator based saturable absorber," *IEEE Photonics J.* **7**, 1–7 (2015).
67. P. G. Yan et al., "Topological insulator solution filled in photonic crystal fiber for passive mode-locked fiber laser," *IEEE Photonics Technol. Lett.* **27**(3), 264–267 (2015).
68. Y. C. Meng et al., "High power L-band mode-locked fiber laser based on topological insulator saturable absorber," *Opt. Express* **23**, 23053–23058 (2015).
69. M. Liu et al., "Microfiber-based, highly-nonlinear topological insulator photonic device for the formation of versatile multi-soliton patterns in a fiber laser," *J. Lightwave Technol.* **33**, 2056–2061 (2015).
70. D. Mao et al., "Soliton fiber laser mode locked with two types of film-based Bi_2Te_3 saturable absorbers," *Photonics Res.* **3**(2), A43–A46 (2015).
71. B. Guo et al., "Observation of bright-dark soliton pair in a mode-locked fiber laser with topological insulator," *IEEE Photonics Technol. Lett.* **27**(7), 701–704 (2015).
72. M. Liu et al., "Dissipative rogue waves induced by long-range chaotic multi-pulse interactions in a fiber laser with a topological insulator-deposited microfiber photonics device," *Opt. Lett.* **40**, 2667–2770 (2015).
73. J. L. Xu et al., "Ultrasensitive nonlinear absorption response of large-size topological insulator and application in low-threshold bulk pulsed lasers," *Sci. Rep.* **5**, 14856 (2015).
74. Y. J. Sun et al., "Passively Q-switched tri-wavelength $\text{Yb}^{3+}:\text{GdAl}_3(\text{BO}_3)_4$ solid-state laser with topological insulator Bi_2Te_3 as saturable absorber," *Photonics Res.* **3**, A97–A101 (2015).
75. H. Ahmad et al., "Tunable S-Band Q-switched fiber laser using Bi_2Se_3 as the saturable absorber," *IEEE Photonics J.* **7**(3), 1 (2015).
76. Q. Wang et al., "Wide spectral and wavelength-tunable dissipative soliton fiber laser with topological insulator nano-sheets self-assembly films sandwiched by PMMA polymer," *Opt. Express* **23**(6), 7681–7693 (2015).
77. L. Gao et al., "Ultrafast pulse mode-locked by topological insulator nanosheets interacting with photonic crystal fiber: from anomalous dispersion to normal dispersion," *IEEE Photonics J.* **7**, 1–8 (2015).
78. B. Guo et al., "Dual-wavelength soliton mode-locked fiber laser with a WS_2 -based fiber taper," *IEEE Photonics Technol. Lett.* **28**(3), 323–326 (2016).
79. W. J. Liu et al., "70-fs mode-locked erbium-doped fiber laser with topological insulator," *Sci. Rep.* **5**, 19997 (2016).
80. P. G. Yan et al., "Multi-pulses dynamic patterns in a topological insulator mode-locked ytterbium-doped fiber laser," *Opt. Commun.* **335**, 65–72 (2015).
81. L. Lu et al., "All-normal dispersion passively mode-locked Yb-doped fiber laser with Bi_2Te_3 absorber," *Opt. Eng.* **54**, 046101 (2015).
82. P. G. Yan et al., "Q-switched fiber laser using a fiber-tip-integrated TI saturable absorption mirror," *IEEE Photonics J.* **8**(1), 1–6 (2016).
83. K. P. Wang et al., "Ultrafast saturable absorption of two-dimensional MoS_2 nanosheets," *ACS Nano* **7**, 9260–9267 (2013).
84. Q. Cui et al., "Transient absorption microscopy of monolayer and bulk WS_2 ," *ACS Nano* **8**, 2970–2976 (2014).
85. S. Wang et al., "Broadband few-layer MoS_2 saturable absorbers," *Adv. Mater.* **26**, 3538–3544 (2014).
86. H. Zhang et al., "Molybdenum disulfide (MoS_2) as a broadband saturable absorber for ultra-fast photonics," *Opt. Express* **22**, 7249–7260 (2014).
87. F. Bonaccorso and Z. P. Sun, "Solution processing of graphene, topological insulators and other 2D crystals for ultrafast photonics," *Opt. Mater. Express* **4**, 63–78 (2014).
88. R. I. Woodward et al., "Tunable Q-switched fiber laser based on saturable edge-state absorption in few-layer molybdenum disulfide (MoS_2)," *Opt. Express* **22**(25), 31113–31122 (2014).
89. R. I. Woodward et al., "Wideband saturable absorption in few-layer molybdenum diselenide (MoSe_2) for Q-switching Yb-, Er- and Tm-doped fiber lasers," *Opt. Express* **23**, 20051–20061 (2015).
90. Y. J. Sun et al., "Comparison of MoS_2 nanosheets and hierarchical nanospheres in the application of pulsed solid-state lasers," *Opt. Mater. Express* **5**, 2924–2932 (2015).
91. Y. J. Sun et al., "Wavelength-tunable, passively Q-switched $\text{Yb}^{3+}:\text{Ca}_3\text{Y}_2(\text{BO}_3)_4$ solid state laser using MoS_2 saturable absorber," *Mater. Lett.* **160**, 268–270 (2015).
92. H. Xia et al., "Ultrafast erbium-doped fiber laser mode-locked by a CVD-grown molybdenum disulfide (MoS_2) saturable absorber," *Opt. Express* **22**, 17341–17348 (2014).
93. J. Du et al., "Ytterbium-doped fiber laser passively mode locked by few-layer molybdenum disulfide (MoS_2) saturable absorber functioned with evanescent field interaction," *Sci. Rep.* **4**, 6346 (2014).
94. R. Khazaiezhad et al., "Mode-locking of Er-doped fiber laser using a multilayer MoS_2 thin film as a saturable absorber in both anomalous and normal dispersion regimes," *Opt. Express* **22**, 23732–23742 (2014).
95. Y. Z. Huang et al., "Widely-tunable, passively Q-switched erbium-doped fiber laser with few-layer MoS_2 saturable absorber," *Opt. Express* **22**, 25258–25266 (2014).
96. Z. Q. Luo et al., "1-, 1.5-, and 2- μm fiber lasers Q-switched by a broadband few-layer MoS_2 saturable absorber," *J. Lightwave Technol.* **32**(24), 4077–4084 (2014).
97. H. Liu et al., "Femtosecond pulse erbium-doped fiber laser by a few-layer MoS_2 saturable absorber," *Opt. Lett.* **39**, 4591–4594 (2014).
98. M. Liu et al., "Microfiber-based few-layer MoS_2 saturable absorber for 2.5 GHz passively harmonic mode-locked fiber laser," *Opt. Express* **22**, 22841–22846 (2014).
99. R. Khazaiezhad et al., "Passively mode-locked fiber laser based on CVD WS_2 ," in *2015 Conf. on Lasers and Electro-Optics (CLEO)* (2015).
100. K. Wu et al., "463-MHz fundamental mode-locked fiber laser based on few-layer MoS_2 saturable absorber," *Opt. Lett.* **40**(7), 1374–1377 (2015).
101. M. Zhang et al., "Solution processed MoS_2 -PVA composite for sub-bandgap mode-locking of a wideband tunable ultrafast Er: fiber laser," *Nano Res.* **8**, 1522–1534 (2015).
102. H. Wang et al., "Ethanol catalytic deposition of MoS_2 on tapered fiber," *Photonics Res.* **3**(3), A102 (2015).
103. D. Mao et al., " WS_2 mode-locked ultrafast fiber laser," *Sci. Rep.* **5**, 7965 (2015).
104. P. G. Yan et al., "Microfiber-based WS_2 -film saturable absorber for ultra-fast photonics," *Opt. Mater. Express* **5**(3), 479–489 (2015).

105. K. Wu et al., "WS₂ as a saturable absorber for ultrafast photonic applications of mode-locked and Q-switched lasers," *Opt. Express* **23**(9), 11453–11461 (2015).
106. M. W. Jung et al., "Mode-locked, 1.94- μ m, all-fiberized laser using WS₂-based evanescent field interaction," *Opt. Express* **23**, 19996–20006 (2015).
107. J. Lin et al., "Wavelength-tunable Yb-doped passively Q-switching fiber laser based on WS₂ saturable absorber," *Opt. Express* **23**, 29059–29064 (2015).
108. P. G. Yan et al., "Passively mode-locked fiber laser by a cell-type WS₂ nanosheets saturable absorber," *Sci. Rep.* **5**, 12587 (2015).
109. A. P. Luo et al., "Few-layer MoS₂-deposited microfiber as highly nonlinear photonic device for pulse shaping in a fiber laser [invited]," *Photonics Res.* **3**, A69–A78 (2015).
110. M. Zhang et al., "Yb- and Er-doped fiber laser Q-switched with an optically uniform, broadband WS₂ saturable absorber," *Sci. Rep.* **5**, 17482 (2015).
111. D. Mao et al., "WS₂ saturable absorber for dissipative soliton mode locking at 1.06 and 1.55 μ m," *Opt. Express* **23**, 27509–27519 (2015).
112. L. Li et al., "WS₂/fluorine mica (FM) saturable absorbers for all-normal-dispersion mode-locked fiber laser," *Opt. Express* **23**, 28698–28706 (2015).
113. P. G. Yan et al., "Self-starting mode-locking by fiber-integrated WS₂ saturable absorber mirror [invited]," *IEEE J. Sel. Top. Quantum Electron.* (2016).
114. B. H. Chen et al., "Q-switched fiber laser based on transition metal dichalcogenides MoS₂, MoSe₂, WS₂, and WSe₂," *Opt. Express* **23**(20), 26723–26737 (2015).
115. S. B. Lu et al., "Broadband nonlinear optical response in multi-layer black phosphorus: an emerging infrared and mid-infrared optical material," *Opt. Express* **23**(9), 11183–11194 (2015).
116. Y. Chen et al., "Mechanically exfoliated black phosphorus as a new saturable absorber for both Q-switching and mode-locking laser operation," *Opt. Express* **23**(10), 12823–12833 (2015).
117. Z. C. Luo et al., "Microfiber-based few-layer black phosphorus saturable absorber for ultra-fast fiber laser," *Opt. Express* **23**, 20030–20039 (2015).
118. J. Sotor et al., "Ultrafast thulium-doped fiber laser mode locked with black phosphorus," *Opt. Lett.* **40**(16), 3885–3888 (2015).
119. J. C. Knight et al., "All-silica single-mode optical fiber with photonic crystal cladding," *Opt. Lett.* **21**, 1547–1549 (1996).
120. P. G. Yan et al., "Double cladding seven-core photonic crystal fibers with different GVD properties and fundamental supermode output," *J. Lightwave Technol.* **31**, 3658–3662 (2013).
121. H. F. Wei et al., "A compact seven-core photonic crystal fiber supercontinuum source with 42.3 W output power," *Laser Phys. Lett.* **10**, 045101 (2013).
122. P. G. Yan et al., "Polarization dependent visible supercontinuum generation in the nanoweb fiber," *Opt. Express* **19**, 4985–4990 (2011).
123. P. G. Yan et al., "Numerical simulation on the coherent time-critical 2-5 μ m supercontinuum generation in an As₂S₃ microstructured optical fiber with all-normal flat-top dispersion profile," *Opt. Commun.* **293**, 133–138 (2013).
124. P. G. Yan et al., "Supercontinuum generation in a photonic crystal fibre," *Chin. Phys. Lett.* **21**, 1093–1095 (2004).
125. L. Wei et al., "Graphene-based Q-switched erbium-doped fiber laser with wide pulse-repetition-rate range," *IEEE Photonics Technol. Lett.* **24**(4), 1853–1855 (2012).
126. H. Mu et al., "Graphene-Bi₂Te₃ heterostructure as saturable absorber for short pulse generation," *ACS Photonics* **2**(7), 832–841 (2015).
127. Y. Q. Jiang et al., "Broadband and enhanced nonlinear optical response of MoS₂/graphene nanocomposites for ultrafast photonics applications," *Sci. Rep.* **5**, 16372 (2015).

Hao Chen is studying for a master's degree at the Shenzhen Key Lab of Laser Technology, Key Laboratory of Advanced Optical Precision Manufacturing Technology of Guangdong Higher Education Institutes, Shenzhen University, China. His current research interests concentrate on passively mode-locked fiber lasers based on topological insulator/few-layer transition-metal dichalcogenides and black phosphorus.

Peiguang Yan received his PhD in the College of Physics Science from Nankai University, China, in 2005. He joined Shenzhen University (China) in 2005 as a lecturer and became an associate professor (2007–2012) and promoted to professor in 2013. His research interests include PCF-based nonlinear fiber optics and passively mode-lock fiber laser by 2D materials. He has authored/coauthored over 50 technical publications.

Biographies for the other authors are not available.